Geological Sequestration of CO2 in Mature Hydrocarbon Fields. Basin and Reservoir Numerical Modelling of the Forties Field, North Sea

J. M. Ketzer, B. Carpentier, Y. Le Gallo, P. Le Thiez

Oil & Gas Science and Technology – Rev. IFP, Vol. 60 (2005), No. 2, pp. 259-273

IFP International Workshop
Rencontres scientifiques de l'IFP

Gas-Water-Rock Interactions ... / Interactions gaz-eau-roche ...

Geological Sequestration of CO_2 in Mature Hydrocarbon Fields

Basin and Reservoir Numerical Modelling of the Forties Field, North Sea

J.M. Ketzer*, B. Carpentier[1], Y. Le Gallo[1] and P. Le Thiez[1]

1 Institut français du pétrole, 1 et 4, avenue de Bois-Préau, 92852 Rueil-Malmaison Cedex - France
e-mail: jm@ketzer.com.br - bernard.carpentier@ifp.fr - yann.le-gallo@ifp.fr - pierre.le-thiez@ifp.fr

*Present address: Universidade Federal do Rio Grande do Sul, Instituto de Geociências, Programa de Geologia do Petróleo, Av. Bento Gonçalves 9500, 91501-970, Porto Alegre - Brazil

Résumé — Piégeage géologique de CO_2 dans un champ d'hydrocarbures mature. Modélisation à l'échelle bassin et réservoir du champ de Forties, mer du Nord — La modélisation numérique est l'un des seuls outils dont on dispose pour évaluer le devenir du CO_2 injecté dans les réservoirs géologiques profonds, et en particulier dans les gisements d'hydrocarbures exploités. Une fois calée sur la situation actuelle observée pour les roches et les fluides, elle peut être utilisée pour prédire la migration du gaz injecté, aussi bien dans le réservoir hôte que dans sa couverture. Nous présentons ici une méthode qui, en utilisant des modèles numériques déjà existants, permet une évaluation des risques de fuite du CO_2 liés à l'environnement géologique. Cette approche a été appliquée à un exemple réel, démontrant l'efficacité du champ de Forties en mer du Nord, vis-à-vis d'un piégeage du CO_2 sur une durée de l'ordre de 1000 a. Nous montrons que les résultats de simulation plaident en faveur d'un comportement favorable à la séquestration. Le temps de résidence calculé pour le CO_2 dépasse largement le millier d'années, ce qui rend ce mode de séquestration du carbone plus durable que beaucoup d'autres. De plus, cette étude contribue à fournir des critères pour définir d'autres champs d'hydrocarbures exploités favorables à la séquestration géologique du CO_2.

Abstract — Geological Sequestration of CO_2 in Mature Hydrocarbon Fields. Basin and Reservoir Numerical Modelling of the Forties Field, North Sea — *Numerical modelling is likely the only available tool to evaluate and predict the fate of CO_2 injected in deep geological reservoirs, and particularly in depleted hydrocarbon fields. Here we present a methodology which aims at evaluating the geological leaking risk of an underground storage using a depleted oil field as the host reservoir. The methodology combines basin and reservoir scale simulations to determine the efficiency of the storage. The approach was designed for the study of the reservoir after the injection of CO_2 and then does not take into account any CO_2 injection period. The approach was applied to the Forties field (North Sea) for which CO_2 behaviour was simulated for a 1000 y time period. Our findings suggest that local geological conditions are quite favourable for CO_2 sequestration. Possible residence time of CO_2 will be in the order of thousands of years and, thus such geological depleted hydrocarbon fields storage is probably a good alternative for a long term CO_2 sequestration. Additionally, results of this work can help to establish criteria to identify other mature hydrocarbon fields aimed for CO_2 sequestration.*

INTRODUCTION

Geological sequestration of CO_2 in mature hydrocarbon fields has been considered as a viable option to reduce accumulation of atmospheric CO_2 and, thus mitigate greenhouse effects on climate (Bradshaw and Cook, 2001). Injection of CO_2 in mature reservoirs might even be economically sustainable because it can enhance oil recovery (Holtz *et al.*, 2001; Stevens *et al.*, 2001). Depleted hydrocarbon reservoirs can store large amounts of CO_2, as the maximum potential storage capacity is considered as the volume of CO_2 that can be disposed from the top of the trap down to the structural spill point (van der Meer, 1992). Therefore, the volume of CO_2 that can potentially be stored in subsurface exceeds that of other sequestration methods such as forestry by three orders of magnitude (Bradshaw and Cook, 2001). Previous studies showed that CO_2 confinement in hydrocarbon reservoirs is more efficient than in aquifers because of the presence of proven traps in the first, which retards CO_2 removal by groundwater flow and leakage through seal, thus increasing its residence time in the reservoir (Machel, this issue). Other promising subsurface CO_2 sequestration methods have been suggested, such as in deep buried coal seams (Steven *et al.*, 2001). Deep coal seams may be economically viable for CO_2 sequestration because of enhanced coal-bed methane recovery and possible sequestration times similar to depleted reservoir (Gale and Freund, 2001).

It is well known that hydrocarbon fields have stored oil and gas for millions of years, however, their efficiency for CO_2 storage is still fairly unknown. Therefore, CO_2 sequestration programs in hydrocarbon fields must consider a complete evaluation of their long-term efficiency to ensure that CO_2 will remain stored for enough time (*e.g.*, thousands of years) to consider the storage process as efficient with respect to climate change. Risk evaluation implies a full understanding of the physical and chemical interactions between CO_2, formation water, and reservoir and cap rocks. CO_2 escape scenarios in mature hydrocarbon fields include: leakage through cap rock, faults and abandoned wells, diffusion in water, and dissolution of CO_2 in water and subsequent transport of CO_2-charged waters in the aquifer, away from the trap. A fast and reliable manner to evaluate the efficiency of the storage is by numerical modelling of the geological system involved. The aim of this paper is to propose a workflow able to evaluate long term geological CO_2 leaking risk by simulating the behaviour of CO_2 in a depleted hydrocarbon field. The methodology, which takes advantage of already available basin and reservoir numerical models was then applied to a real field case. The late Paleocene sandstones of the Forties field, North Sea, was selected by *BP* as a good candidate to be such field case. The Forties Field was selected because of the availability of suitable input data (well logs, 2D and 3D seismic), absence of large faults, and good sealing capacity of its cap rock. This work is part of a more comprehensive European Union program named NGCAS (Next Generation CO_2 Capture and Storage) that aims to assess the risks of geological storage of CO_2 in mature hydrocarbon fields for, at least, 1000 y. Therefore, here we investigate the capacity of the Forties field to store CO_2 for the next 1000 y. This study will ultimately contribute for a complete risk assessment of CO_2 storage in the Forties field. We will not discuss in this paper loss or mineral trapping of CO_2 owing to chemical interactions with water, rocks and well cements.

For the simulations, we assumed that the CO_2 injection has been completed and that the maximum filling of the pore space was reached with supercritical CO_2, from the top of the structure to its spill point. The CO_2 saturation has been set to a high, but still realistic value of 0.5. This initial CO_2 distribution (before any leakage) in the Forties reservoir was defined from gas injection simulation performed by *ECL Technology Ltd* within the NGCAS project. This "water alternate gas" (WAG) injection study was conducted using the VIP compositional simulation model (*BP*) on a sector of the Forties Charlie sand. The model was initially waterflooded and then subjected to WAG with CO_2 as the injection gas. A range of simulations were performed to investigate different WAG strategies. The maximum volume of CO_2 sequestered in the reservoir was around 50% of the hydrocarbon pore volume. After injection gas moved upwards until trapped under shales or at the top of the reservoir.

1 METHODOLOGY

The ideal approach to assess the potential risks of CO_2 leakage from a depleted hydrocarbon field is to model the field in detail using a 3D model. However, because the present day and future fluid conditions in and around the field (pressures, temperature, water flow, etc.) depend on the whole history of the basin, the evaluation of the present basin conditions, needs, theoretically, a total modelling of the basin evolution from its origin to present day. Such 3D model is very difficult to complete because of the usual lack of precise geological data.

To overcome this difficulty, we defined a multi-scale approach comprising four stages:

1 Long basin scale cross-sections leading the potential water charge areas (outcrops) to the deep part of the basin and passing through the studied field. These regional cross-sections, usually based on long seismic lines provide information on the water flows around the field and is used to define boundary conditions for the field scale 3D simulation.

2 Simulation of the fluid flow in the field and its surrounding drainage area using 3D basin modelling (Temis 3D) and the boundary conditions defined in stage 1.

3 Simulation, at reservoir scale, of the interaction between CO_2 and water (diffusion) using an *IFP* fluid flow simulator (Simuscopp).
4 Sensitivity study on the fluid flow parameters (mainly permeability and capillary pressure) in order to evaluate the maximum risk of CO_2 leakage. These calculations, where the reservoir and cap-rock permeability can be increased by a factor of 100, allows to quantify the maximum leakage of CO_2 and thus to evaluate its maximum environmental risk.

This paper presents an application of the above approach on the Forties Field with the aim to compute the CO_2 escape routes and quantify the CO_2 transfer to the underlying aquifer and the overburden once the CO_2 is in place within the Forties field.

According to the above work-flow, a regional 2D cross-section was used to quantify the water charges around the Forties area. Then, using these boundary conditions and the 3D Temis model, flow pattern was calculated to determine pressure boundary conditions for reservoir simulations performed by the *IFP* Simuscopp code, numerical code which, at the difference with Temis, is able to take into account CO_2 diffusion in water.

2 STUDY AREA AND GEOLOGICAL SETTING

The study was developed in an area of 50 × 31 km encompassing the Forties field. The Forties field is a mature oil field, discovered in 1970 and in production since 1975, located in the central North Sea at 180 km ENE offshore Aberdeen, Scotland *(Fig. 1)*. Water depth in the study area ranges from 80 to 140 m.

The Forties field (Paleocene reservoir) consists of a dome structure, about 90 km^2 in area, with a vertical relief of 180 m. Measured temperature in the reservoir is about 90°C, and pressure is close to hydrostatic. The original oil-water contact was at 2217 m depth (pressure ≈ 22.67 MPa), and coincided approximately with the depth of the structural spill point. Oil is moderately mature, light, low-sulphur, medium-wax, and was sourced from the Jurassic Kimmeridge clay formation (Wills and Peattie, 1990). Migration occurred during the middle Eocene to Miocene, and late Eocene to present-day (Wills and Peattie, 1990). There are no large faults present in the reservoir and the minor faults encountered are believed to have no significant influence on reservoir continuity or production (Wills and Peattie, 1990).

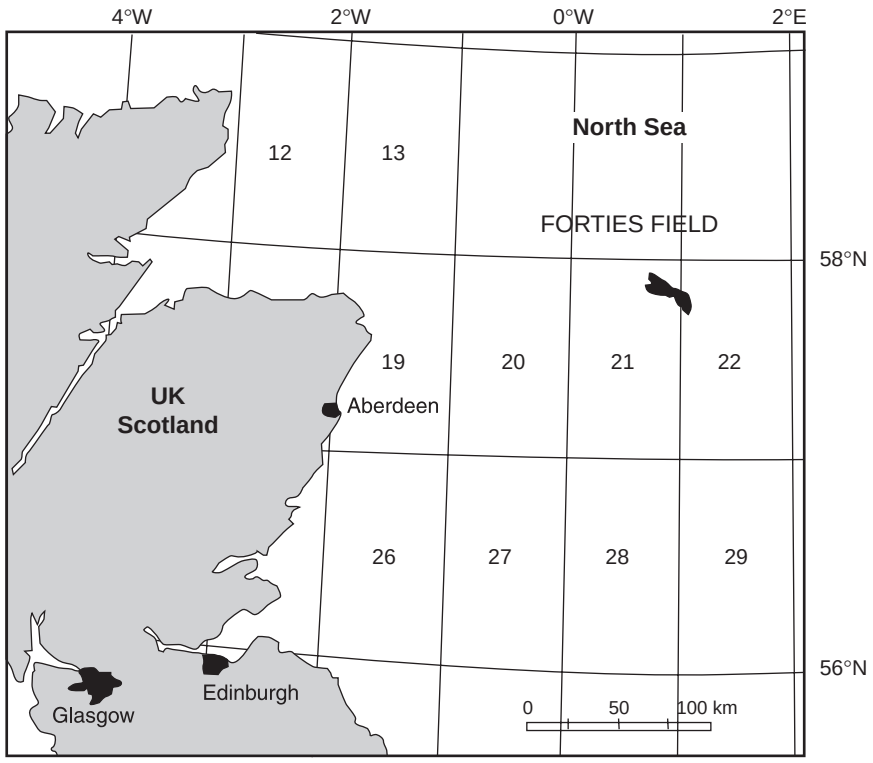

Figure 1

Location map of the study area (Forties field).

Reservoir rocks are Thanetian (late Paleocene), channel and interchannel turbidite, poorly lithified, sublithic to lithic sandstones of the Forties formation (Morton, 1987; Wills and Peattie, 1990). These rocks are part of an extensive, Paleocene sand-rich submarine fan system (the Forties fan) that also includes the Maureen and Lista formations *(Fig. 2)*. The Forties fan was deposited on top of late Cretaceous and Danian mudstones, limestones and chalk (Hill and Wood, 1980) of the Tor and Ekofisk formations, respectively *(Fig. 2)*. The deposition of the Forties fan terminated at the end of the late Paleocene, and was succeeded by the deposition of mudstones of the Sele and Balder formations (early Eocene). The first forms the regional top seal to the Forties reservoir. From the Eocene to the Holocene, there is a thick (≈ 2 km) sequence of dominantly mudstones and siltstones, with rare interbedded sandstones, of the Hordaland and the Nordland groups (Glennie, 1998; *Fig. 2*).

Group	Formation (member)	Lithology	Period/Epoch
Nordland Hordaland		Mudstones and siltstones	Holocene to late Eocene
Moray	Balder Sele	Mudstones	Early Eocene
	Forties	Sandstones	Late Paleocene
Montrose	Lista Lista (Balmoral) Lista (Andrew) Maureen	Sandstones	Early to late Paleocene
Chalk	Ekofisk	Chalk	
	Tor	Mudstones and limestones	Late Cretaceous

Figure 2

Chart showing the lithostratigraphic framework of the study interval (late Cretaceous to Holocene).

3 MATERIAL AND METHODS

According to the above defined work-flow, our modelling work comprised a multi-scale approach with three distinct phases.

Phase 1 consists on the construction of a regional cross section from basin margin to basin centre, that passed through or close by the Forties oil field. The section needed to detail the geometry of key geological horizons, with a particular emphasis on sandy stratigraphic units and the connectivity of these with the Forties reservoir rocks. A seismic profile from a speculative survey shot by *WesternGeco* was chosen to provide this information, passing within 20 km of the Forties field. It is 250 km long and data quality is good. The profile is oriented approximately EW, from a position 42 km off the coast of NE Scotland near Fraserburgh, eastwards into Norwegian waters. It passes through or close by many key hydrocarbon wells and hence geological control on the interpretation of reflectors is good. This work was performed within the NGCAS project by supervision of T. Bidstrup from the *Geological Survey of Denmark and Greenland (GEUS)* and S. Holloway from the *British Geological Survey*. This important work will not be developed in this paper but the result shows that:

– Two almost separate pressure systems exist in the Forties area;
  - a Jurassic-lower Cretaceous system which is related to grabens with tight shale and active hydrocarbon systems;
  - a Paleocene/Neogene system of which the Forties sand is a part. Pressure changes in the Jurassic of 20 MPa only generate a pressure change in the fan sand of 0.3 MPa, demonstrating the small degree of communication between the two systems. This important results allowed us, in the case of Forties, to simplified the 3D study to the Paleocene/Neogene geological system even if the modelling of the maturation of the Jurassic source-rock and hydrocarbon filling history of Forties would have been a good way to demonstrate, by mass balance, the capacity of Forties to retain a large proportion of the generated hydrocarbons.
– The potential range of pressures in the Forties sands along strike from the Forties field may vary from almost hydrostatic (zero overpressure) to maximum overpressure of 3.5 MPa.
– The pressure boundary conditions for the 3D modelling should be close to hydrostatic and that the pressure gradient across the field should lie between 0 MPa/100 km and 1 MPa/100 km.

Phase 2 consisted of basin scale (tens of kilometres) modelling, and aimed at calculating the regional water flow around and into the Forties field. For this phase, we used the commercial Temis 3D 2.0 basin modelling software, which is able to calculate water flow vectors (velocities and directions) at basin scale. It assumes a fluid movement according to the Darcy's law. Detailed information about the principles of Temis 3D can be found in Schneider *et al.*, (2000 and references therein), and thus will not be presented here. This type of model has to be used because it is able to calculate fluid displacement in taking into account the change in layer thickness related to geological compaction. However, it has to be considered only a "preprocessor" for reservoir type simulator such as Simuscopp because it is not able to take into account water-oil-gas interactions such as diffusion processes which is of paramount importance for CO_2 escape.

Phase 3, as already explained, consisted of reservoir scale (kilometres) modelling—not very different from the Temis 3D model—which aimed at simulating the dissolution and diffusion of CO_2 into formation water, as well as flow of CO_2 through the cap rock and overburden interval. For this phase we use *IFP*'s Simuscopp code, which is able to simulate 3D multi-phase and multi-component fluid flow, dissolution and diffusion. Principles, equations and a validation of Simuscopp code can be found in Le Thiez *et al.* (1996).

Materials used for this work were provided by *BP*, and include:

– ten topographic maps for layer boundaries between the Cretaceous and Holocene *(Fig. 3)*, each map corresponding to a seismic reflector that has been traced in several 2D seismic lines, and linked with true depths in well logs;
– 3D block encompassing the whole Forties reservoir with lithological data (porosity, permeability) from seismic inversion;
– data on forty-six wells, containing lithological description and wire line logs.

4 THREE-D BASIN SCALE MODELLING

The basin scale modelling followed five steps: block building, gridding, boundary conditions setting, and backward (backstripping) and forward simulations. Block building consisted in creating a 3D block around the Forties field, comprising the area defined for this study (50 × 31 km), extending in depth from the sea floor, down to the base Cretaceous at 4730 to 2457 m depth. The block comprised nine layers with boundaries and geometry defined by ten top and base topographic maps *(Fig. 3)*.

Lithology maps were created for each of the nine layers *(Fig. 4)*. These maps were elaborated from lithological descriptions available for all studied wells. For the reservoir interval, we complemented the lithology maps based on well logs with lithology information from inversion of the 3D seismic block. These maps were created by loading both the Temis 3D block with lithology maps from well logs, and the inverted seismic 3D block, in the gOcad® software. The lithology information from the inverted block was then transferred into the Temis 3D block by using gOcad®'s Transfer Property tool. In order to incorporate the high resolution lithology data from the seismic inversion in the model, we subdivided the original nine layers into thirty-one extra layers, particularly in the reservoir interval. The geometry of these intermediate layers was defined by intermediate topographic maps obtained by linear interpolation of the original topographic maps.

A total of sixteen lithology types were created *(Table 1)*, and lithology properties (*e.g.*, solid density, thermal conductivity) were obtained either from default Temis 3D values or by mixing two lithology types using Temis 3D New Mix Lithology tool. Porosity vs. depth curves were either from default Temis 3D lithology types or extracted from literature (Giles, 1997 and references therein). Permeability for all lithologies was calculated from specific surface area and porosity, using the modified Kozeny-Carman law, as follows:

$$k = \frac{0.2\,\Phi^m}{S^2(1-\Phi)^2}$$

where Φ is porosity, m is the "tortuosity" of the porous media, and S is the specific surface area (*i.e.*, the ratio of surface area to volume of matrix solid). All lithologies properties used in the simulations are listed on Table 1.

After block building, we defined an optimum grid tacking into account the compromise between cell size (resolution of input data) and total number of cells in the model (CPU time/hardware capacity). In this study we used a regular grid with the maximum number of cells possible for the available hardware. At the end of the simulation (last event) the number of cells was 441 600, distributed in a grid with 120 × 90 cells in the horizontal plan and 40 layers. Each cell was approximately 400 × 400 m large in the horizontal plan, and of height equal to the respective layer thickness.

Before starting the simulations, pressure boundary conditions (hydrostatic, closed for fluid flow or any given pressure), in time, for all block faces need to be set. The top face (sea floor) is considered hydrostatic, while the bottom face is assumed to be closed (no fluid flow). The precise boundary conditions for the other four vertical block faces (north, south, east and west) are difficult to establish. Recent regional studies in the North Sea Basin suggest that there is a pressure gradient coupled with regional groundwater flow in the Paleocene sands (including the Forties formation), from the depocentre of the basin at SE to the Forties field at NW, where pressures are equilibrated to hydrostatic (Evans *et al.*, 2003). To simulate such a NW regional groundwater flow, it was decided to establish boundary conditions as follows: hydrostatic for North and West faces, and closed for South and East faces, but with a 20 m head for the reservoir interval *(Fig. 5)*. Other simulation parameters assumed were: water density 1030 kg/m^3, surface temperature 12°C, and geothermal gradient 30°C/km. Heat production of rock was neglected and the thermal conductivity of geological layers are assumed to be isotropic. Permeability is isotropic in the horizontal plane and anisotropic in the vertical direction (see *Table 1*).

In addition to the simulation described above hereafter referred to as "base case" and in accordance to step four of our risk assessment methodology, we performed sensibility tests in which permeability (both of the reservoir and overburden), and boundary conditions of the base case have been changed to encompass other scenarios in which parameters might have been under- or overestimated, because of poor quality control data, such as in the overburden (*Table 2*). These tests allow us to take into account the uncertainties

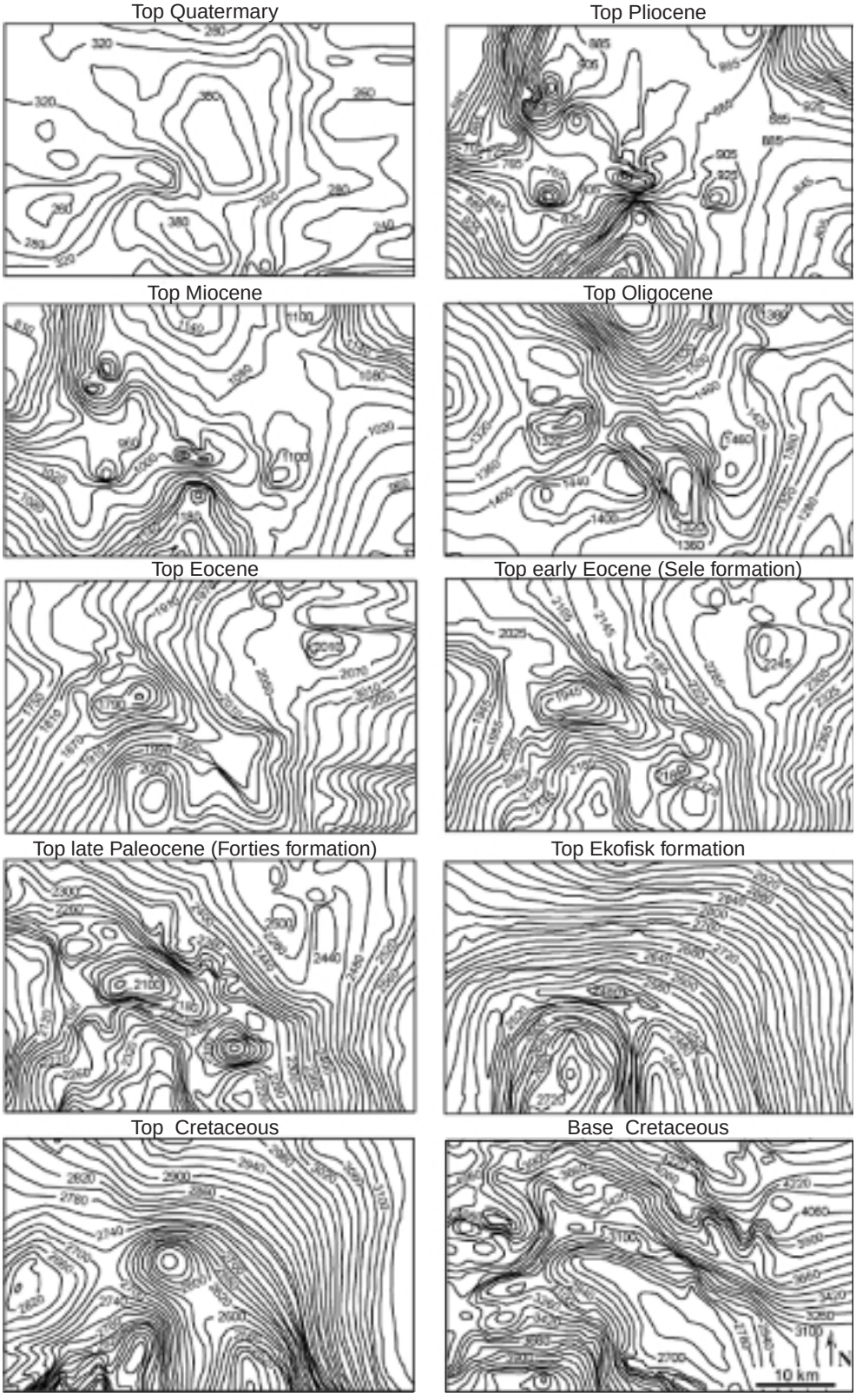

Figure 3

Isobathic maps used to define top and base of each model layer. Origin of all maps (lower left corner) at UTM coordinates 360 050 and 6 385 050. Line interval is 20 m for all maps, except for base Cretaceous map (80 m).

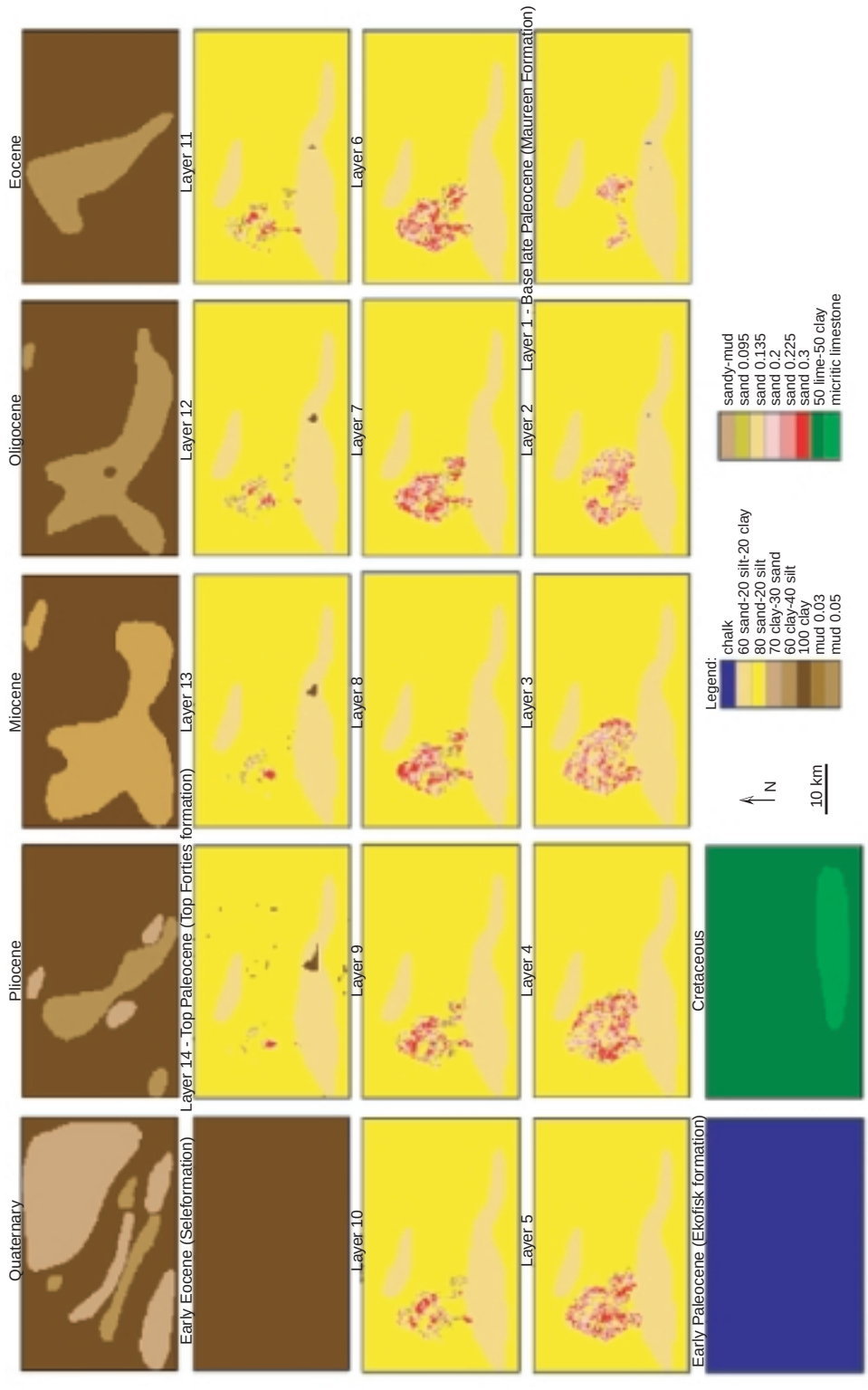

Figure 4

Lithology maps constructed from well logs (Quaternary, Pliocene, Miocene, Oligocene, Eocene, early Eocene, early Paleocene, and Cretaceous), and from well logs and 3D seismic inversion (layers 1-14).

TABLE 1

Main physical properties used for each of the sixteen lithology types included in the modelling

	Sand 0.3*	**Sand 0.255***	**Sand 0.2***	**Sand 0.135***	**Sand 0.095***	**Sandy-Mud***	**80sand-20silt**	**60sand-20silt-20mud**	**70clay-30sand**	**60clay-40silt**	**100clay**	**Mud 0.05***	**Mud 0.03***	**50lime-50clay**	**Micritic limestone**	**Chalk**
Solid density ***(kg/m^3)***	2650	2650	2650	2680	2680	2755	2650	2680	2755	2750	2800	2750	2750	2754	2708	2700
Thermal parameters																
Conductivity																
20°C (W/m/°C)	2.5	2.5	2.5	2.5	2.5	2.5	2.5	2.5	2.5	2.5	1.8	2.5	2.5	2.5	2.5	3.25
Temperature dependency (1/°C)	0.001	0.001	0.001	0.001	0.001	0.001	0.001	0.001	0.001	0.001	1.0E-4	1.0E-4	1.0E-4	0.001	1.0E-4	3.0E-4
Horizontal multiplier	1	1	1	1	1	1	1	1	1	1	1	1	1	1	1	1
Vertical multiplier	1	1	1	1	1	1	1	1	1	1	1	1	1	1	1	1
Mass heat capacity (J/kg/°C)	1000	1000	1000	1000	1000	1000	1000	1000	1000	1000	840	1000	1000	1000	1000	960
Rradiogeneic production	0	0	0	0	0	0	0	0	0	0	0	0	0	0	0	0
Porosity																
minimum value	0.05	0.05	0.05	0.04	0.04	0.02	0.05	0.04	0.02	0.03	0.02	0.03	0.03	0.03	0.01	0.02
porosity A	0.091	0.0122	0.0293	0.1842	0.367	0.067	0.0087	0.057	0.177	0.1137	0.1431	0.0027	0.0064	0.1502	0.4079	0.3119
sigma A (MPa)	1	1	3.3748	14.7758	10.6102	1.314	1	3.1601	3.2138	2.2104	1.7983	9.5533	8.482	4.371	1	12.0842
porosity B	0.4109	0.4078	0.3907	0.3358	0.153	0.5426	0.463	0.4113	0.433	0.5563	0.5369	0.6673	0.6636	0.3798	0.2881	0.3681
sigma B (MPa)	33.5627	30.383	27.3349	16.0653	28.7605	13.7217	25.0646	21.4318	18.9908	16.2228	13.1628	9.6223	8.5168	20.8464	9.6744	12.0862
Elasticity (MPa)	10,000	10,000	10,000	10,000	10,000	10,000	10,000	10,000	10,000	10,000	1,000	10,000	10,000	10,000	1,000	1,000
Porosity vs. depth (m)																
	0-0.47 125-0.45 250-0.425 500-0.385 1,000-0.35 1,500-0.33 2,000-0.31 3,000-0.25 5,000-0.1	0-0.47 125-0.45 250-0.425 500-0.385 1,000-0.35 1,500-0.3 2,000-0.27 3,000-0.21 5,000-0.08	0-0.47 125-0.45 250-0.425 500-0.385 1,000-0.33 1,500-0.28 2,000-0.22 3,000-0.17 5,000-0,08	0-0.56 125-0.53 250-0.5 500-0.43 1000-0.35 1500-0.25 2000-0.15 3000-0.1 5,000-0.6	0-0.56 125-0.53 250-0.5 500-0.43 1,000-0.3 1,500-0.22 2,000-0.15 3,000-0.1 5,000-0.06	0-0.63 125-0.57 250-0.51 500-0.42 1,000-0.3 1,500-0.2 2,000-0.1 3,000-0.06 5,000-0.04	0-0.47 125-0.45 250-0.425 500-0.385 1,000-0.33 1,500-0.28 2,000-0.225 3,000-0.16 5,000-0.08	0-0.56 125-0.53 250-0.5 500-0.43 1,000-0.35 1,500-0.28 2,000-0.21 3,000-0.14 5,000-0.06	0-0.63 125-0.57 250-0.51 500-0.42 1,000-0.3 1,500-0.2 2,000-0.15 3,000-0.08 5,000-0.04	0-0.7 125-0.65 250-0.6 500-0.5 1,000-0.37 1,500-0.275 2,000-0.18 3,000-0.1 5,000-0.03	0-0.7 125-0.625 250-0.55 500-0.44 1,000-0.285 1,500-0.175 2,000-0.115 3,000-0.045 5,000-0.02	0-0.7 125-0.65 250-0.6 500-0.5 1,000-0.33 1,500-0.18 2,000-0.07 3,000-0.05 5,000-0.03	0-0.7 125-0.65 250-0.6 500-0.5 1,000-0.3 1,500-0.12 2,000-0.04 3,000-0.03 5,000-0.03	0-0.56 125-0.51 250-0.47 500-0.39 1,000-0.28 1,500-0.2 2,000-0.16 3,000-0.09 5,000-0.04	0-0.796 125-0.35 250-0.3 500-0.248 1,000-0.19 1,500-0.163 2,000-0.149 3,000-0.14 5,000-0.12	0-0.7 125-0.65 250-0.6 500-0.5 1,000-0.35 1,500-0.23 2,000-0.175 3,000-0.08 5,000-0.02
Permeability																
Fracturing threshold	0	0	0	0	0	0	0	0	0	0	1	0	0	0	1	0
Specific area (m^2/m^3)	75,000	75,000	75,000	1.0E+05	1.0E+05	5.0E+06	75,000	1.0E+05	5.0E+06	1.0E+7	1.0E+8	1.0E+8	1.0E+8	2.0E+7	1.0E+7	5.0E+06
Horizontal multiplier	1	1	1	1	1	1	1	1	1	1	1	1	1	1	1	1
Vertical multiplier	1	0.7	0.7	0.5	0.5	0.2	0.7	0.5	0.2	0.2	0.1	0.1	0.1	0.2	1	1

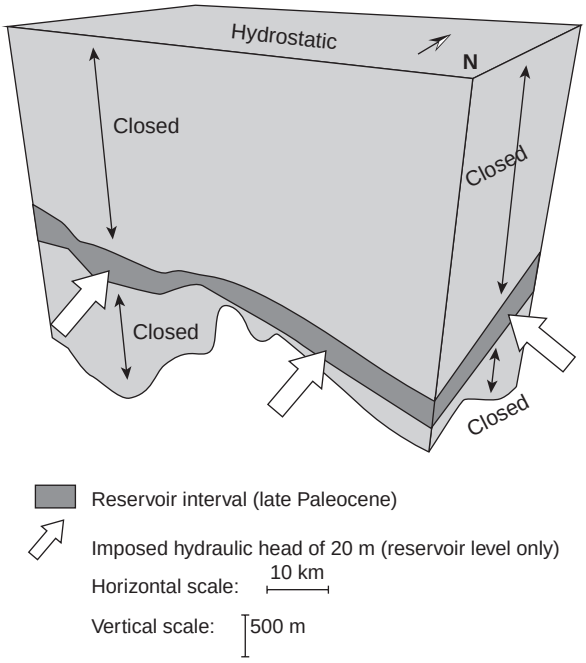

Figure 5

Boundary conditions for the basin scale model. Note that pressure conditions for North and West block faces are set to hydrostatic.

which are always associated with geological data. As a matter of fact, in our approach, and this is true for the Temis 3D simulation as for the Simuscoop simulations which will be described in details hereafter, we did not try to better define the critical parameters which control the fluid flows, we just increase or decrease arbitrary these parameters by several orders of magnitude and see what are their effects on the fluid behaviour. If in the worth case (maximum permeability, maximum water flow and minimum capillary pressure) the CO_2 leakage still stays negligible, we would have demonstrated that the risk of CO_2 leakage is very low for the considered storage site.

5 THREE-D RESERVOIR SCALE MODELLING

The reservoir scale modelling consisted of three phases: block building, initial conditions setting, and simulation. The reservoir model (geometry, and lithology properties such as porosity) was derived from the basin scale block. Using Temis 3D upscaling tool, we cut a block with 24.9×24.5 km, encompassing all the Forties field area, with an origin at the UTM coordinates 366 360 and 6 388 075, extending in depth from the sea floor, down to the base Cretaceous at 4730 to 2457 m depth *(Fig. 6).* This block was then imported into gOcad® software, and exported in ASCII format, compatible with Simuscopp.

In this study, the Simuscopp block comprises a regular grid with 311 040 cells, distributed in a grid with 96×81 cells in the horizontal plan and 40 layers *(Fig. 6).* Each cell was approximately 300×300 m large in the horizontal plane, and of height equal to the respective layer thickness. Hydrostatic boundary conditions were used for all the four vertical (north, south, east, west) block faces, based on results of the basin scale simulations.

Initial conditions for simulations included:

- complete filling of the reservoir from the top of the structure up to the original oil water contact, at 2217 m and 22.67 MPa, with supercritical CO_2;
- CO_2 saturation of 0.5 (*i.e.*, 638.2 10^6 m^3 or 390 Mt of CO_2 injected);
- water density of 1030 kg/m^3 and salinity of 35 g/l;

TABLE 2

Combination of parameters (boundary conditions, reservoirs permeability and overburden permeability) used in each of the12 sensibility cases of the basin scale model

Boundary conditions	Reservoir permeability		Overburden permeability			Overburden and reservoir permeability
	× 10	× 1	× 10	× 0.1	× 0.01	× 10
S-E closed N-W hydrostatic	Case 9	Case 3				
S-E 20 m head N-W hydrostatic	Case 8	**Base case**	Case 1	Case 5	Case 2	Case 10
S-E 30 m head N-W hydrostatic		Case 4				
S-E 50 m head N-W hydrostatic	Case 11	Case 6				Case 12
S-E closed N-W hydrostatic for Forties but closed for overburden		Case 7				

– two phases (water and gas) and two components (H_2O and CO_2);
– reservoir temperature of 90°C;
– simulation time of 1000 y.

The CO_2 gas-liquid equilibrium is based on Duan *et al.* (1992), gas phase volumetric properties are based on the Peng-Robinson equation of state (T_C = 30.95°C, P_C = 73.8 bar, acentric factor = 0.239 from Reid *et al.*, 1987), gas (CO_2) phase viscosity uses the Lohrenz-Bray-Clark model. An uniform tortuosity (set to 1) was applied in the model, and diffusion in the water phase is derived from the Tyn and Calus correlation (10^{-4} m^2/d; Reid *et al.*, 1987).

To simplify petrophysical (relative permeability and capillary pressure) rock type description in the simulations, we used only two types of lithology, sandstone and mudstone, for definition of compressibility, relative permeability and capillary pressure concerns. Figure 7 shows relationships used for relative permeability and capillary pressure computation. Compressibility for sandstone was 4.35 10^{-5} bar^{-1}, while for mudstone it was 10^{-5} bar^{-1}.

In addition to the simulation described above, we run a sensibility test for the reservoir scale model, in which we neglected capillary (and pore entry) pressure for cap rock and overburden mudstones. Pore entry pressure represents the required pressure to enter the largest pore in the rock. Thus, the CO_2 flow was controlled primarily by the permeability of the rocks. As capillary pressure prevents CO_2 migration from the reservoir to the cap rock (except by diffusion in the water phase), this was considered as a worst case scenario for CO_2 sequestration in the Forties field.

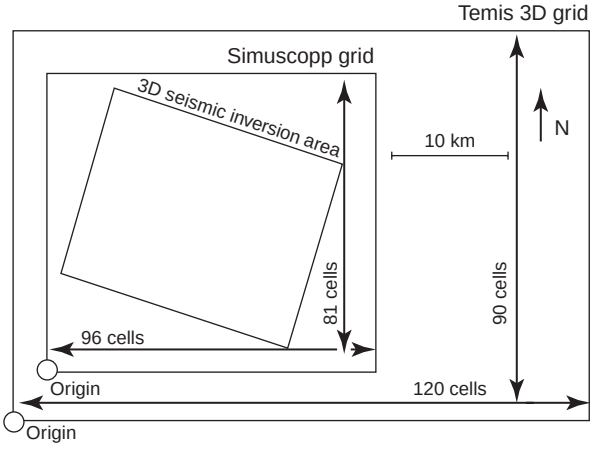

Figure 6

Grids for basin scale (Temis 3D) and reservoir scale (Simuscopp) models. Note the location of the 3D seismic inversion block.

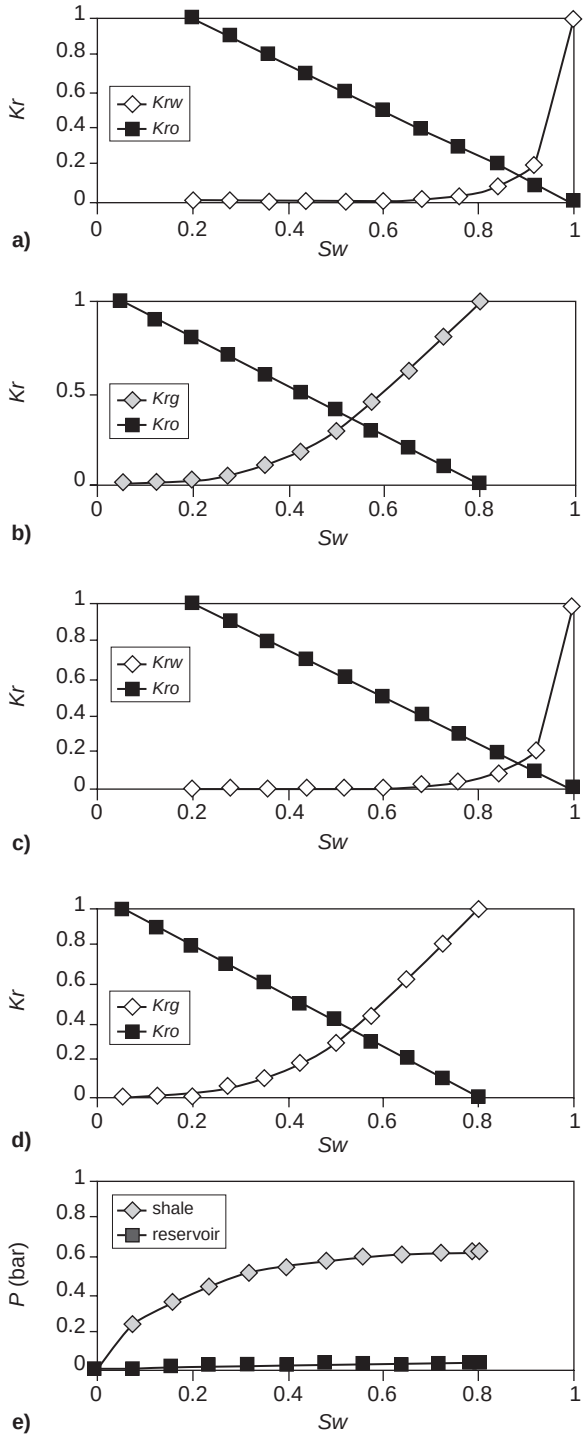

Figure 7

Parameters used in the reservoir scale model: a) relative permeabilities (*Kr*) of water (*Krw*) and oil (*Kro*) for sandstone; b) relative permeabilities of oil (*Kro*) and gas *Krg*) for sandstone; c) relative permeabilities of water (*Krw*) and oil (*Kro*) for mudstone; d) relative permeabilities of oil (Kro) and gas (*Krg*) for mudstone; and e) pore entry pressure (*P*) for sandstones and mudstones. *Sw* and *Sg* refer to water and gas saturations, respectively.

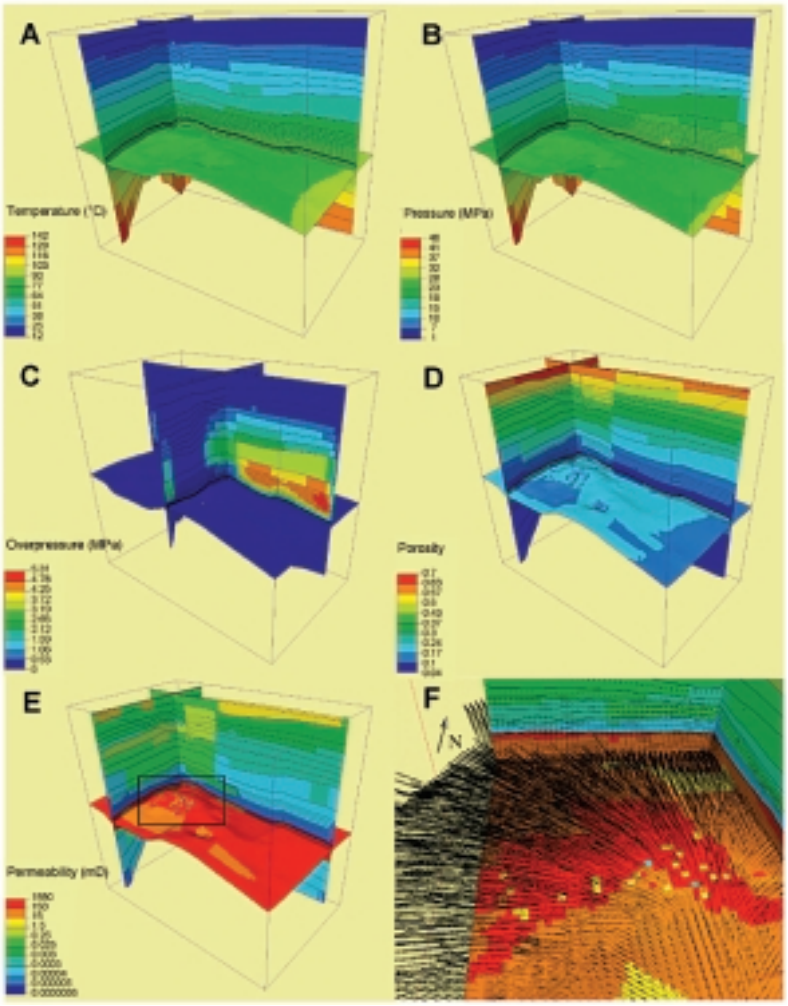

Figure 8

Results of basin scale modelling (present-day situation) showing distribution of: (A) temperature; (B) pressure; (C) overpressure; (D) porosity; (E) permeability; and (F) water flow vectors in the reservoir level are black arrows pointing mainly to Northwest. Flux is proportional to the length of the arrows (maximum length = 500 m/Ma). Diagram F is a magnification of the area marked by the black frame on diagram E.

6 RESULTS

6.1 Basin Scale Simulations

Basin scale simulation resulted in the following range of values for the Paleocene sandstones, which are consistent with the available data for the Forties field and physical processes involved in the basin evolution: pressure 21-30.5 MPa, overpressure 0-0.0001 MPa, temperature 71-90°C, porosity 0.13-0.27, horizontal permeability 45-1250 mD, and vertical permeability 20-1000 mD *(Fig. 8).* The present-day fluid flow at the basin scale shows a complex geometric pattern, with about 80% of the total flow restricted to the Paleocene sandstones. Present-day pressure distribution varies with depth, lithology, and imposed boundary conditions. Our simulations revealed an overall decrease in pressure from SE to NW, and a consequent water flow from SE to NW, with a dominant horizontal component *(Fig. 8f).* In the top of the Paleocene sandstones, close to the Eocene mudstones (cap rock), however, flow is mainly downwards, while in the base, close to the early Tertiary and late Cretaceous limestones and mudstones, flow is predominantly upwards. The small difference in overpressure in the Paleocene sandstones (< 0.0001 MPa, *i.e.*, nearly hydrostatic as also observed in recent regional studies in the North Sea Basin for the Paleocene sands, cf. Evans *et al.*, 2003) resulted in very low present-day water flow rates (< 575 m/Ma). This flow rate is the slowest value calculated for the Paleocene sandstones since deposition of the overburden deposits, in the Eocene. Peak values were reached during the Oligocene

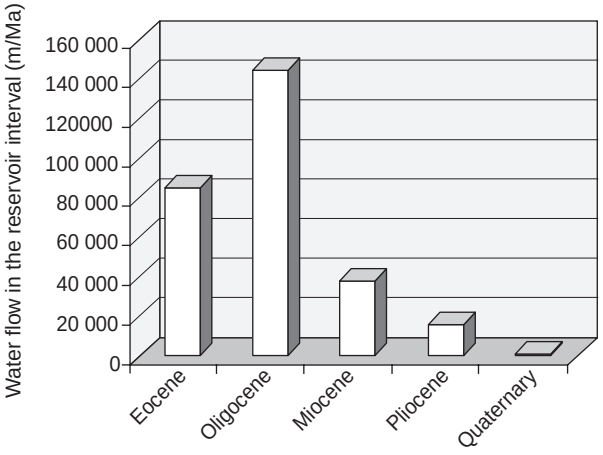

Figure 9

History of fluid flow in the reservoir interval calculated from the basin scale modelling (bars represent maximum fluid flow values).

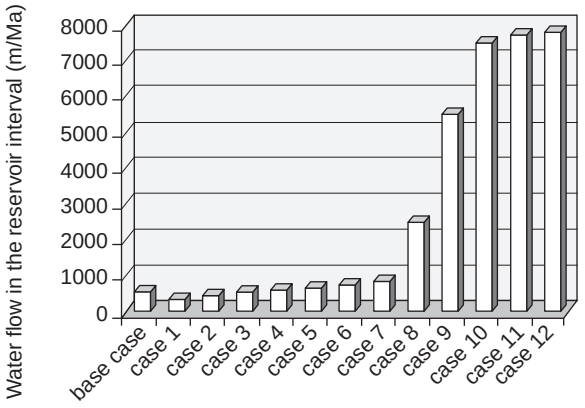

Figure 10

Results of fluid flow calculated from the basin scale model for the base case and sensibility tests (cases 1-12), for present-day conditions.

(up to 145 000 m/Ma), with an abrupt decrease in the Miocene up to the Quaternary *(Fig. 9)*.

Overpressures in the overburden interval are up to 5.3 MPa, and mainly located in the centre and South and Eastern parts of the model, approximately between 1800 and 2300 m depth. In the centre of the model overpressure drops to less than 1 MPa (*Fig. 8c*). Water flow in the upper overburden interval (0 to ≈ 1400 m depth) is less than 60 m/Ma in mudstones and less than 150 m/Ma in siltstones, with flow vectors oriented predominantly upwards. In the lower overburden interval (> 1400 m depth) water flow is < 10 m/Ma in the mudstones and less than 30 m/Ma in the siltstones, with flow vectors oriented predominantly downwards. Water flow in the interval below the Paleocene sandstones (upper Cretaceous and Danian) is less than 10 m/Ma in all lithology types.

The different sensibility tests performed starting from the base case resulted in moderate changes (one order of magnitude) in the groundwater flow rates in the Paleocene sandstones (*Fig. 10*). There are no significant changes in the orientation of the regional water flow, from South-East to North-West, in all sensibility tests. Pressure calculated in the Paleocene sandstones was always near hydrostatic (overpressure < 0.01 MPa) for all performed sensibility tests. In the overburden, however, overpressure reached values of 8 and 11 MPa (cases 6 and 2), where permeability of the overburden was multiplied by 0.1 and 0.01, respectively.

6.2 Reservoir Scale Simulations

Reservoir scale simulation shown that small amounts of sequestered supercritical CO_2 moved upwards (by diffusion and flow), out of the trap, through the cap rock *(Fig. 11)*. Only 3.6% of the original mass of CO_2 injected in the Forties field escaped the trap over the 1000-year period of simulation *(Fig. 12a)*. Our simulations show that after 100 y, CO_2 is still trapped in the reservoir, and no leakage is observed. At 250 y, however, CO_2 started to move upwards and penetrated the first 50 m of the cap rock mainly by diffusion, with saturations between *(Fig. 11)* 0.05 (top) and 0.11 (base). At 500 y, CO_2 is still in the first 50 m in the cap rock, but reached slightly higher saturation values (0.11 in the top, and 0.14 in the base). After 700 y, the CO_2 plume continues to move upwards and reached 90 m in the cap rock. At this stage, saturation varied between 0.05-0.08 at the top, and 0.11-0.14 at the base *(Fig. 11)*. At the end of the simulation, after 1000 y, CO_2 moved 135 m into the cap rock, and saturation has reached 0.05 at the top, and 0.14 at the base *(Fig. 11)*.

The simulation with no capillary pressure for mudstones revealed that almost 37% of the original mass of CO_2 has migrated out of the trap *(Fig. 12b)*. In this case, after 100 y, CO_2 started already to move upwards and penetrated the first 50 m of the cap rock, with saturations between 0.05-0.08 (top) and 0.05-0.26 (base). At 250 y, CO_2 reached 90 m into the cap rock, with saturations between 0.05 (top) and 0.05-0.26 (base). After 500 y, the CO_2 plume continued to move upwards and reached 135 m of the cap rock. At this stage, saturation varied between 0.05-0.08 at the top, and 0.08-0.38 at the base. At 750 y, CO_2 is still in the first 135 m in the cap rock, but reached slightly higher saturation in a larger area (0.08 in the top, and 0.38 in the base). At the end of the simulation, after 1000 y, CO_2 had moved 220 m into the cap rock, and saturation had reached 0.05 at the top, and 0.08-0.041 at the base.

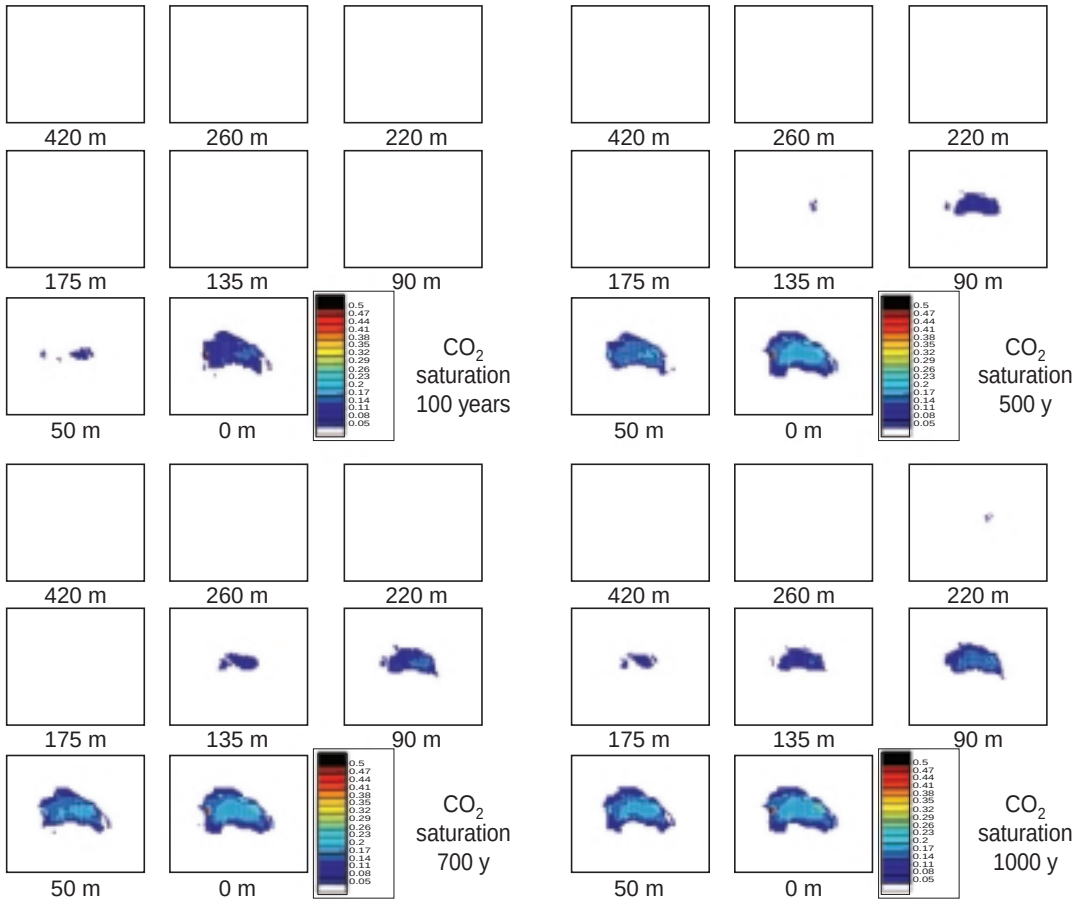

Figure 11

Evolution of the pore saturation of CO_2 in 100, 500, 700, and 1000 y after injection, in a succession of maps in the overburden units (sealing), calculated from the reservoir scale model. Numbers below maps are distances above the crest of the reservoir structure.

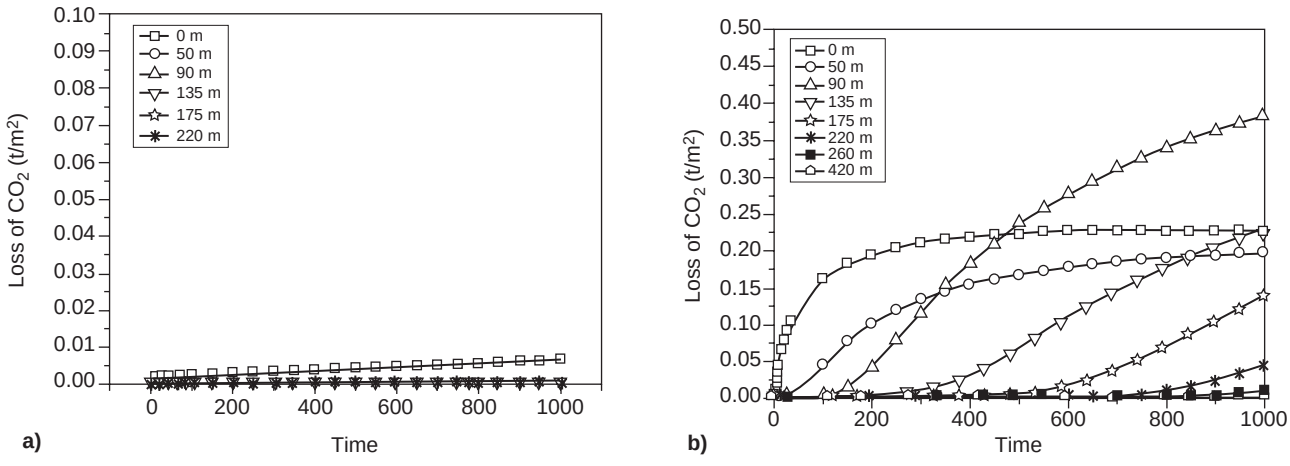

Figure 12

Graphics showing loss of CO_2 from the reservoir, calculated from the reservoir scale model. Lines represent results for different distances above the crest of the reservoir structure. a) is for base case and b) is for sensibility test (neglected pore entry pressure).

DISCUSSION

The present-day fluid flow pattern (magnitude and orientation of flow vectors) encountered in the Forties field region is typical of sedimentary basins under compactional regimes (Galloway, 1984; Giles, 1997). The calculated flow rate in the Paleocene sandstones (< 575 m/Ma) is within the range expected for sediments at depths greater than 2000 m, where most of the water has been already expelled, and pore pressure is close to hydrostatic (Giles, 1997). As the modelled area is close to such equilibrium, there is little chance to significantly increase flow rates in the Paleocene sandstones by compaction of the overburden. Changes in flow rates, caused by changes in the tectonic regime, for instance, are unlikely to operate on a time-scale of 1000 y.

The very low flow rate in the Paleocene sandstones (< 575 m/Ma) indicates that, even with complete dissolution of CO_2 in groundwater immediately after injection, CO_2-charged waters will not be displaced significantly (< 1 m) from their initial position within the Forties reservoir, in the next 1000 y. Even the worst case scenario simulated (sensibility test case 12), in which flow rates reached c.a. 8000 m/Ma, CO_2-charged waters will be displaced over distances less than 8 m in the next 1000 y. Hence, there is no immediate risk (next thousands of years) for CO_2 to escape by dissolution and diffusion in the groundwater, and transportation through the aquifer (Paleocene sandstones) away from the Forties field.

Reservoir scale simulation indicates that, although CO_2 moved upwards in the cap rock, it did so at very low rates and mainly through diffusion in water. Therefore, the CO_2 plume travelled only a small distance (135 m) in the overburden in the 1000 y of simulation, when compared to the burial depth of the Forties field (≈ 2 km). Even in the case where no capillary pressure was considered, the CO_2 reached only 220 m above the crest of the reservoir structure. This is, in part, attributed to the good sealing capacity of the cap rock (*i.e.*, its low permeability). Additionally, the dominance of low permeability rocks in the overburden (mainly mudstones and siltstones) would aid in delaying upward movement of CO_2 after it has pass through the cap rock.

Another important point to consider is that there are no significant quantities of CO_2 removed from the reservoir in the 1000 y of simulation (3.6% of the original mass), as shown by the generally very low saturation values observed in the cap rock (≈ 0.08).

CONCLUSIONS

The basin and reservoir scales numerical models of the Forties field presented here showed that local geological conditions, such as good sealing capacity of the cap rock (*i.e.*, low permeability), compactional regime close to hydrostatic equilibrium (below 2 km depth), overburden dominated by mudstones and siltstones, and absence of faults, are quite favourable for CO_2 sequestration. Such criteria can be used to aid selection of other mature hydrocarbon fields aimed for CO_2 sequestration.

Basin scale simulation revealed very low groundwater flow rates for the Paleocene reservoir rocks (< 575 m/Ma), indicating that there is no risk for significant removal of CO_2 by groundwater flow in the aquifer, for the next 1000 y. Sensibility tests showed that, even in the worst case scenario modelled (flow rates ≈ 8000 m/Ma), groundwater flow still cannot lead to significant removal of CO_2 from the reservoir.

Reservoir scale simulations indicate that, although CO_2 moved upwards into the cap rock, its displacement in the next 1000 y is relatively small (< 135 m) compared to the burial depth of the Forties field (≈ 2 km). Additionally, CO_2 saturation levels reached at the top of the plume are fairly low (< 0.05). Simulation of a worst case scenario, in which we neglected capillary (pore entry) pressure, which prevents CO_2 moving from the reservoir into the cap rock, revealed that CO_2 plume will move only 220 m upwards in the overburden, because of the presence of low permeability rocks (dominantly mudstones).

Our findings suggest that residence time of CO_2 in the Forties field will be of the order of thousands of years and thus will be much longer lasting than other available carbon sequestration methods. However, additional processes resulting from CO_2 sequestration in the Forties field not taken into account for in the present work should also be considered in risk analysis. Risks for CO_2 sequestration in the Forties field, not taken into account in this work include:

- CO_2 escape via abandoned wells;
- CO_2 dissolution of the reservoir and/or cap rocks owing to chemical interactions between dissolved gas and minerals.

Future work on chemical CO_2-water-rock interactions may quantitatively explain precipitation and dissolution of reservoir and/or cap rocks, and possible permanent CO_2 sequestration via mineral trapping.

ACKNOWLEDGEMENTS

The authors thank other participants of NGCAS (Next Generation CO_2 Capture and Storage) project, especially Steven Cawley (*BP*), Mike Sauders (*BP*), Torben Bidstrup (*GEUS*), Gary Kirby (*British Geological Survey*), for discussions and constructive comments during all stages of this work. We also thank *BP* for allowing access to well logs, core descriptions and structural maps of the Forties field area. The authors gratefully acknowledge the funding and support given by the *EU Commission Directorate-General for Energy and Transport (TREN)*, and the CO_2 Capture Project (*CCP*). Anonymous reviewers and editors John Lynch and Étienne Brosse are acknowledge for their constructive comments on the manuscript. J. Marcelo Ketzer thanks *IFP* and the head of the *Division of Geology and Geochemistry*, Bernard Colleta, for a post-doctoral grant.

REFERENCES

Bradshaw, J. and Cook, P. (2001) Geological sequestration of carbon dioxide. *Environmental Geosciences*, 8, 149-151.

Crawford, R., Littlefair, R.W and Affleck, L G. (1991) The Arbroath and Montrose fields, blocks 22/17, 18, UK North Sea. 211-217 in United Kingdom Oil and Gas Fields, 25 Years Commemorative Volume. Abbots, I L, (editor). *Memoir of the Geological Society of London*, **14**.

Duan, Z. *et al.* (1992) An equation of state for the CH_4-CO_2-H_20 system: I. Pure systems from 50 to 1000°C and from 0 to 8000 bar. *Geochimica et Cosmochimica Acta*, **56**, 2605-2617.

Evans, D., Graham, C., Armour, A. and Bathurst, P. (2003) *The Millennium Atlas: Petroleum Geology of the Central and Northern North Sea*, The Geological Society of London, London.

Gale, J., and Freund, P. (2001) Coal-bed methane enhancement with CO_2 – Sequestration worldwide potential. *Environmental Geosciences*, **8**, 210-217.

Galloway, W.E. (1984) Hydrogeologic regimes of sandstone diagenesis, in *Clastic Diagenesis* MacDonald, D.A. and Surdam, R.C. (eds.), *American Association of Petroleum Geologists Memoir*, **37,** Tulsa, 3-14.

Giles, M.R. (1997) *Diagenesis: A Quantitative Perspective*, Kluwer Academic Plublishers, Dordrecht.

Glennie, K.W. (1998) *Petroleum Geology of the North Sea – Basic Concepts and Recent Advances*, Blackwell Sciences, Oxford.

Hill, P.J., and Wood, G.V. (1980) Geology of the Forties Field, U.K. Continental Shelf, North Sea. In: *Giant Oil and Gas Fields of the Decade 1968-1978*, Halbouty, M.T. (ed.), *American Association of Petroleum Geologists Memoir*, **30**, Tulsa, 81-93.

Holtz, M.H., Nance, P.K., and Finley, R.J. (2001) Reduction of greenhouse gas emissions through CO_2 EOR in Texas. *Environmental Geosciences*, **8**, 187-198.

Le Thiez, P.A., Pottecher, G., and Côme, J.M. (1996) Validation of a general 3-D numerical model for simulating organic pollutants migration and application to site remediation. *International Conference on Health, Safety and Environment*, *Society of Petroleum Engineers*, Louisiana, 9-12 June, 723-733.

Morton, A.C. (1987) Influences on provenance and diagenesis on detrital garnet suites in the Paleocene Forties sandstone, central North Sea. *Journal of Sedimentary Petrology*, **57**, 1027-1032.

Reid, R.C., Prausnitz, J.M., *et al.* (1987) *The Propeties of Gases and Liquids*, Mc Graw-Hill Book Company, London.

Schneider, F., Wolf, S., Faille, I., and Pot, D. (2000) A 3D basin model for hydrocarbon potential evaluation: application to Congo offshore. *Oil & Gas Science and Technology – Revue IFP*, **55**, 3-13.

Stevens, S.H., Kuuskraa, V.A., Gale, J. and Beecy, D. (2001) CO_2 injection and sequestration in depleted oil and gas fields and deep coal seams: worldwide potential and costs. *Environmental Geosciences*, **8,** 200-209.

van der Meer, L.G.H. (1992) Investigations regarding the storage of carbon dioxide in aquifers in the Netherlands. *Energy Conversion and Management*, **33**, 611-618.

Wills, F.M., and Peattie, D.K. (1990) The Forties Field and the evolution of a reservoir management strategy. In: *North Sea Oil and Gas Reservoirs-II*, Buller, A.T., Berg, E., Hjelmeland, O., Kleppe, J., Torsaeter, O., and Aasen, J.O. (eds.), The Norwegian Institute of Technology, Graham & Trotman, 1-18.

Final manuscript received in December 2004